Analytical Solutions for Circular Bars Subjected to Large Strain Plastic Torsion

K. W. Neale
Faculty of Applied Science,
Université de Sherbrooke,
Sherbrooke, QC, Canada
Assoc. Mem. ASME

S. C. Shrivastava
Department of Civil Engineering and Applied Mechanics,
McGill University,
Montréal, QC, Canada

The inelastic behavior of solid circular bars twisted to arbitrarily large strains is considered. Various phenomenological constitutive laws currently employed to model finite strain inelastic behavior are shown to lead to closed-form analytical solutions for torsion. These include rate-independent elastic-plastic isotropic hardening J_2 flow theory of plasticity, various kinematic hardening models of flow theory, and both hypoelastic and hyperelastic formulations of J_2 deformation theory. Certain rate-dependent inelastic laws, including creep and strain-rate sensitivity models, also permit the development of closed-form solutions. The derivation of these solutions is presented as well as numerous applications to a wide variety of time-independent and rate-dependent plastic constitutive laws.

1 Introduction

In recent years much attention has been focused on the development of constitutive laws for elastic-plastic solids, especially with regard to the modeling of finite strain behavior. Generally the aim has been to produce phenomenological theories which adequately model the essential features of material response, yet which remain simple enough for numerical applications. This has usually been achieved by appropriately extending the classical small strain theories of plasticity to the large strain regime. Examples of this approach are the finite strain versions of J_2 flow theory of plasticity, proposed by Budiansky (1970) and Hutchinson (1973) for isotropic hardening, and subsequently modified by Tvergaard (1978) for kinematic hardening, as well as the hypoelastic and hyperelastic versions of J_2 deformation theory of Stören and Rice (1975) and Hutchinson and Neale (1978a). Extensions of such models to include the effects of material strain-rate sensitivity have also been proposed (Hutchinson and Neale (1978b)).

The kinematic hardening law first suggested by Tvergaard (1978) was a plausible finite strain generalization of the classical Prager-Ziegler rule of small strain plasticity. However, for simple shear deformations this law was shown to predict strongly oscillatory shear stresses (Nagtegaal and de Jong, 1982). To eliminate such oscillations, various modified kinematic hardening rules have been advanced (e.g., Lee et al., 1983; Dafalias, 1983).

A fundamental problem related to finite strain constitutive modeling is the behavior of solid circular bars in torsion. Interest in this problem stems from the fact that the torsion test is perhaps the most widely used for obtaining experimental data for metals at very large strains. In addition, the nonhomogeneity of this deformation process and the inherent nonproportional stressing histories involved are prime sources of interest into the basic mechanics of this problem.

In previous investigations of large strain torsion (Neale and Shrivastava, 1985, 1989) numerical results have been generated assuming rate-independent, elastic-plastic, isotropic hardening J_2 flow theory of plasticity (Budiansky, 1970; Hutchinson, 1973), the various kinematic hardening rules of flow theory (Tvergaard, 1978; Lee et al., 1983; Dafalias, 1983), and both the hypoelastic (Stören and Rice, 1975) and hyperelastic (Hutchinson and Neale, 1978a) formulations of J_2 deformation theory. We have since recognized that closed-form analytical solutions can, in many instances, be obtained for the inelastic behavior of solid circular bars twisted to arbitrarily large strains. For example, most of the aforementioned constitutive laws permit the development of such closed-form solutions. Certain rate-dependent inelastic laws, including creep and strain-rate sensitivity models, also lead to closed-form solutions for torsion. The derivation of these solutions is given in this paper, as well as numerous applications to a wide variety of time-independent and rate-dependent constitutive laws. The conditions which render a particular constitutive model amenable to such closed-form solutions for large strain torsion are also discussed.

2 Analysis and Method of Solution

We consider a homogeneous, incompressible solid circular bar of radius R subjected to an angle of twist ψ per unit length. The bar is constrained axially, thus allowing the possible development of axial stresses and a resultant axial force F. The lateral surface of the bar is traction free, and all properties are assumed to be axisymmetric. Although some of the con-

Contributed by the Applied Mechanics Division of THE AMERICAN SOCIETY OF MECHANICAL ENGINEERS for publication in the JOURNAL OF APPLIED MECHANICS.

Discussion on this paper should be addressed to the Technical Editor, Leon M. Keer, The Technological Institute, Northwestern University, Evanston, IL 60208, and will be accepted until two months after final publication of the paper itself in the JOURNAL OF APPLIED MECHANICS. Manuscript received by the ASME Applied Mechanics Division, October 10, 1988; final revision, July 1, 1989.

stitutive models to be considered give rise to deformation-induced anisotropies, the behavior in all cases remains axisymmetric.

A spatial cylindrical polar coordinate system (θ, z, r) with orthonormal base vectors $\mathbf{e}_\theta$, $\mathbf{e}_z$, $\mathbf{e}_r$ is used as a reference. These base vectors are associated with material elements in their current, deformed state so that the various components of stress, rate-of-deformation, etc., in what follows represent the respective physical components.

The kinematics of the above-posed torsion problem is readily determined. The deformation field is such that material points with coordinates (Φ, z, r) in the initial, undeformed configuration currently have coordinates (θ, z, r) in the deformed state, with $\theta=\Phi+\psi z$. Accordingly, the (Eulerian) rate-of-deformation tensor ($\dot{\epsilon}$) and material spin tensor (ω) are such that

$$\dot{\epsilon}_{\theta z}=\dot{\epsilon}_{z\theta}=\omega_{\theta z}=-\omega_{z\theta}=\frac{\dot{\gamma}}{2}\ , \tag{1}$$

where $\dot{\gamma}=r\dot{\psi}$. Thus, each element of the bar is in a state of simple shear in the $\theta-z$ plane, where the shear deformation γ is directly proportional to the radial distance r. That is,

$$\gamma(r)=\frac{r}{R}\,\Gamma \tag{2}$$

where $\Gamma=R\psi$ represents the shear at the outer radius of the bar.

Because of axisymmetry and the prescribed boundary conditions, the only equation of equilibrium which is not identically satisfied is the relation

$$r\frac{d\sigma_{rr}}{dr}+\sigma_{rr}-\sigma_{\theta\theta}=0\ , \tag{3}$$

where σ_{ij} is the Cauchy stress tensor. Furthermore, we have $\sigma_{r\theta}=\sigma_{rz}=0$ throughout the bar.

For simple shear deformations, the various constitutive models to be employed allow us to obtain explicit expressions for the deviatoric stress components s_{ij} as a function of γ (and $\dot{\gamma}$ for rate-dependent behavior). To this state an arbitrary hydrostatic pressure p can be superimposed. Since

$$\sigma_{ij}=s_{ij}-\delta_{ij}p\ , \tag{4}$$

where δ_{ij} is the Kronecker delta, the equilibrium equation (3) becomes

$$\frac{dp}{dr}=\frac{ds_{rr}}{dr}+\frac{1}{r}(s_{rr}-s_{\theta\theta}). \tag{5}$$

Solving this, together with the boundary condition $\sigma_{rr}(R)=0$, gives the hydrostatic pressure distribution $p(r)$. Combining the pressure $p(r)$ with the previously determined stress deviator distributions $s_{ij}(\gamma(r))$ and using (2) and (4) gives the total stress distributions $\sigma_{ij}(r)$. The resultant torque T and axial force F are given by

$$T=2\pi\int_0^R r^2\sigma_{z\theta}dr \tag{6}$$

and

$$F=2\pi\int_0^R r\sigma_{zz}dr\ , \tag{7}$$

respectively. Obviously, since $\sigma_{z\theta}=s_{z\theta}$ the hydrostatic pressure has no influence on T.

For each of the constitutive models to be used we have $s_{rr}=0$, or $\sigma_{rr}=-p$. As a result, the boundary condition becomes $p(R)=0$ and the solution to (5) is

$$p(r)=-\int_R^r\frac{1}{r}\,s_{\theta\theta}(\gamma)dr\ . \tag{8}$$

In equation (8), $s_{\theta\theta}(\gamma)$ is the stress deviator component from the simple shear analysis at $\gamma=r\Gamma/R$ (and $\dot{\gamma}=r\dot{\Gamma}/R$ for rate-dependent behavior).

Since $s_{rr}=0$, we have $s_{zz}=-s_{\theta\theta}$ or $\sigma_{zz}=-(s_{\theta\theta}+p)$. Substituting this and (8) in (7) and integrating by parts gives

$$F(\Gamma)=-\frac{3\pi R^2}{\Gamma^2}\int_0^\Gamma\gamma s_{\theta\theta}(\gamma)d\gamma. \tag{9}$$

Equation (6) can also be written as

$$T(\Gamma)=\frac{2\pi R^3}{\Gamma^3}\int_0^\Gamma\gamma^2 s_{z\theta}(\gamma)d\gamma. \tag{10}$$

Thus, for a bar twisted to a shear deformation Γ at its outer radius, the simple shear solution $s_{ij}(\gamma)$ together with (9) and (10) immediately give the axial force and twisting couple, without recourse to solving explicitly for the pressure distribution $p(r)$. However, to obtain the corresponding stress distributions $\sigma_{ij}(r)$ across the bar, the pressure distribution must be evaluated using (8).

3 Constitutive Models of Time-Independent and Rate-Dependent Plasticity

A number of models of time-independent and rate-dependent large strain plasticity will be considered. These include rigid-plastic and elastic-plastic forms of J_2 flow theory, with isotropic hardening and kinematic hardening, as well as hypoelastic and hyperelastic versions of J_2 deformation theory. Classical creep laws and certain models of material strain-rate sensitivity will also be employed. The various constitutive laws are summarized in this section. Throughout, incompressibility is assumed. Cartesian axes, with x_1, x_2, x_3 associated with the $\mathbf{e}_\theta$, $\mathbf{e}_z$, $\mathbf{e}_r$ directions in torsion, are used as a reference.

3.1 Isotropic Hardening J_2 Flow Theory. For this model the plastic strain-rate components are related to the stress deviator tensor as follows

$$\dot{\epsilon}_{ij}^p=\frac{\dot{\gamma}_e^p}{2\tau_e}\,s_{ij}. \tag{11}$$

Here, $\tau_e=(s_{ij}s_{ij}/2)^{1/2}$ and $\dot{\gamma}_e^p=(2\dot{\epsilon}_{ij}^p\dot{\epsilon}_{ij}^p)^{1/2}$ are the equivalent shear stress and plastic shear strain rate, respectively. These are related to the usual uniaxial equivalent stress (σ_e) and axial plastic strain rate ($\dot{\epsilon}_e{}^P$) through $\tau_e=\sigma_e/\sqrt{3}$ and $\dot{\gamma}_e{}^P=\sqrt{3}\dot{\epsilon}_e{}^P$, where σ_e and ϵ_e reduce to the uniaxial true stress and logarithmic strain for simple tension.

Elastic effects are incorporated by adding the components

$$\dot{\epsilon}_{ij}^e=\frac{1}{2G}\overset{*}{s}_{ij}, \tag{12}$$

where G is the elastic shear modulus. The asterisk denotes the Jaumann rate which, for any second-order tensor, $\mathbf{T}$, and antisymmetric spin tensor, $\boldsymbol{\Omega}$, is related to the material rate, $\dot{\mathbf{T}}$, through

$$\overset{*}{\mathbf{T}}=\dot{\mathbf{T}}+\mathbf{T}\boldsymbol{\Omega}-\boldsymbol{\Omega}\mathbf{T}. \tag{13}$$

For rigid-plastic behavior the total stress deviator components are, from (11),

$$s_{ij}=\frac{2\tau_e}{\dot{\gamma}_e}\dot{\epsilon}_{ij}. \tag{14}$$

For elastic-plastic response, inverting the sum of (11) and (12) gives the incremental relation

$$\overset{*}{s}_{ij}=2G\dot{\epsilon}_{ij}-\frac{1}{\tau_e{}^2}(G-G_t)s_{ij}s_{kl}\dot{\epsilon}_{kl}. \tag{15}$$

Here, G_t is the tangent shear modulus, that is the slope of the equivalent shear stress—shear strain curve at the current level $\tau=\tau_e$. Similarly, in (14) τ_e is regarded as a function of γ_e and can be computed at the current value of γ_e using the

equivalent shear stress—shear strain curve. Equivalently, the uniaxial true stress (σ_e) – logarithmic strain (ϵ_e) curve in simple tension could be used where $\sigma_e = \sqrt{3}\tau_e$, $\epsilon_e = \gamma_e/\sqrt{3}$ and the tangent modulus is $E_t = 3G_t$.

3.2 Kinematic Hardening J_2 Flow Theory. With this model the initial yield surface retains its shape and size but translates in stress space during plastic deformation. The current yield surface is given by

$$\frac{1}{2}\bar{s}_{ij}\bar{s}_{ij} = \tau_Y^2 = \text{const.}, \tag{16}$$

where

$$\bar{s}_{ij} = s_{ij} - \beta_{ij}. \tag{17}$$

Here, β_{ij} specifies the current position of the yield surface origin in deviatoric stress space and τ_Y is the initial yield stress in shear, equal to $\sigma_Y/\sqrt{3}$ where σ_Y is the tensile yield stress.

For elastic-plastic behavior the relation analogous to (15) becomes (Tvergaard, 1978)

$$\overset{*}{s}_{ij} = 2G\dot{\epsilon}_{ij} - \frac{1}{\tau_Y^2}(G - G_t)\bar{s}_{ij}\bar{s}_{kl}\dot{\epsilon}_{kl}. \tag{18}$$

Tvergaard (1978) proposed that G_t be computed at the stress level

$$\tau_e = \tau_Y + (\beta_e)_{\max} \tag{19}$$

where $\beta_e = (\beta_{ij}\beta_{ij}/2)^{1/2}$.

Alternatively, (but not equivalently!) G_t has been taken as a function of the von Mises equivalent plastic strain γ_e^p (as defined in rate form in the previous subsection) and computed from the equivalent shear stress—shear strain curve at the value γ_e^p (Nagtegaal and de Jong, 1982; Lee et al., 1983; Dafalias, 1983). The first alternative will be employed here.

The yield surface translation during an increment of plastic deformation is given by the Prager-Ziegler shift rule

$$\overset{*}{\beta}_{ij} = \bar{s}_{ij}\dot{\mu}\,, \quad \dot{\mu} > 0 \tag{20}$$

which, together with (18) and the consistency condition $\dot{\tau}_Y = 0$, gives

$$\dot{\mu} = \frac{1}{2\tau_Y^2}\bar{s}_{ij}\overset{*}{s}_{ij} = \frac{G_t}{\tau_Y^2}\bar{s}_{ij}\dot{\epsilon}_{ij}. \tag{21}$$

For the rigid-plastic case we have (c.f. equation (14))

$$\bar{s}_{ij} = \frac{2\tau_Y}{\dot{\gamma}_c}\dot{\epsilon}_{ij} \tag{22}$$

with $\dot{\gamma}_c = (2\dot{\epsilon}_{ij}\dot{\epsilon}_{ij})^{1/2}$. The expressions (20) and (21) simplify and can be conveniently written as

$$\overset{*}{\beta}_{ij} = 2G_t\dot{\epsilon}_{ij}. \tag{23}$$

The various kinematic hardening models (e.g., Tvergaard, 1978; Lee et al., 1983; Dafalias, 1983) differ only in the choice of spin tensor Ω used in the definition (13) of the Jaumann rate. These are detailed in Section 4.2.

3.3 Hypoelastic J_2 Deformation Theory. According to the hypoelastic version of finite strain J_2 deformation theory (Stören and Rice, 1975) we have, in incremental form,

$$\overset{*}{s}_{ij} = 2G_s\dot{\epsilon}_{ij} - \frac{1}{\tau_e^2}(G_s - G_t)\, s_{ij}s_{kl}\dot{\epsilon}_{kl}. \tag{24}$$

Here, τ_e is the equivalent shear stress, as defined in Section 3.1, and $G_s = \tau_e/\gamma_e$ is the secant shear modulus, computed from the equivalent shear stress—shear strain curve at the level τ_e. Note that (24) reduces to the isotropic hardening flow theory relation (15) when we put $G_s = G$. In the initial elastic range, we have $G_s = G_t = G$ and (24) reduces to the relation (12).

3.4 Hyperelastic J_2 Deformation Theory. The deformation theory of Hutchinson and Neale (1978a) represents a nonlinear elastic law which is truly path independent for arbitrarily large strains. It makes extensive use of Hill's (1970) theory for finitely deformed isotropic elastic solids. For such solids the principal directions of Cauchy stress must be aligned with the principal directions of Eulerian strain. Thus, to fully specify the constitutive behavior for an incompressible material we need only know the relations between the principal Cauchy stress deviators s_i and corresponding principal stretches λ_i. These are given by

$$s_i = \frac{2\tau_e}{\gamma_e}\epsilon_i \tag{25}$$

where $\epsilon_i = ln\lambda_i$ are the principal components of logarithmic strain, and $\tau_e = (s_i s_i/2)^{1/2}$ as previously. However, γ_e is now defined in terms of the total principal logarithmic strains as $\gamma_e = (2\epsilon_i\epsilon_i)^{1/2}$. The relationship between τ_e and γ_e is again that described by the equivalent shear stress—shear strain curve.

3.5 Rate Dependent Plasticity Laws. The relations that are often used to describe creep deformations or material strain-rate sensitivity are viscoplastic generalizations of the previous rate-independent models. For example, (14), i.e.,

$$\dot{\epsilon}_{ij} = \frac{\dot{\gamma}_e}{2\tau_e}s_{ij} \tag{26}$$

with $\tau_e = (s_{ij}s_{ij}/2)^{1/2}$, $\dot{\gamma}_e = (2\dot{\epsilon}_{ij}\dot{\epsilon}_{ij})^{1/2}$ and $\dot{\gamma}_e = k\tau_e^n$ (27)

is the classical nonlinear viscous creep law (Odqvist, 1966). Hutchinson and Neale (1978b) incorporate strain-rate sensitivity in (14) and (26) by taking τ_e to be a function of γ_e and $\dot{\gamma}_e$ as follows:

$$\tau_e = K\gamma_e^N\dot{\gamma}_e^m. \tag{28}$$

Here, N and m are the strain hardening exponent and strain-rate sensitivity index, respectively. This expression reduces to (27) when $N=0$ and $m = 1/n$. Other equivalent shear stress—strain—strain-rate expressions of the form

$$\tau_e = \mathfrak{F}(\gamma_e, \dot{\gamma}_e) \quad \text{or} \quad \dot{\gamma}_e = \mathfrak{G}(\tau_e, \gamma_e) \tag{29}$$

may be adopted.

4 Solutions for Large Strain Torsion

As outlined in Section 2, knowing the stress deviator components s_{ij} as functions of γ in simple shear (and $\dot{\gamma}$ for rate-dependent behavior) is the key to the development of an analytical solution for the solid bar in torsion, as each element in the bar is in a state of simple shear (in the θ-z plane) with a superimposed hydrostatic pressure. The pressure distribution across the bar is given by (8), the stress components by (4), and the resultant axial force and twisting couple by (9) and (10), respectively.

4.1 Isotropic Hardening J_2 Flow Theory. For simple shear deformations (1), the elastic-plastic isotropic hardening flow theory law (15) leads to the following relations:

$$s_{\theta\theta} = -s_{zz}\,, \quad s_{rr} = s_{r\theta} = s_{rz} = 0 \tag{30}$$

$$\tau_e = (s_{\theta\theta}^2 + s_{z\theta}^2)^{1/2} \tag{31}$$

$$\dot{s}_{\theta\theta} = \left(1 - \frac{G - G_t}{\tau_e^{\,2}}s_{\theta\theta}\right)s_{z\theta}\dot{\gamma} \tag{32}$$

$$\dot{s}_{z\theta} = \left(G - s_{\theta\theta} - \frac{G - G_t}{\tau_e^{\,2}}s_{z\theta}^2\right)\dot{\gamma} \tag{33}$$

The initial "elastic" (in fact, hypoelastic) response corre-

sponding to (12) is obtained by putting $G_t = G$ in the above relations. The solution of the resulting equations is

$$s_{\theta\theta} = -s_{zz} = 2G\sin^2\frac{\gamma}{2}, \quad s_{z\theta} = G\sin\gamma. \tag{34}$$

Plastic yielding occurs when $\tau_e = 2G\sin(\gamma/2) = \tau_Y$, i.e., when

$$\gamma = \gamma_Y = 2\sin^{-1}\left(\frac{\tau_Y}{2G}\right). \tag{35}$$

To obtain a solution in the elastic-plastic range ($\gamma \geq \gamma_Y$), we introduce a parametric angle α as follows such that (31) becomes automatically satisfied:

$$s_{\theta\theta} = \tau_e\sin\alpha, \quad s_{z\theta} = \sigma_{z\theta} = \tau_e\cos\alpha. \tag{36}$$

Substituting (36) into (32) and (33) and solving for $\dot{\tau}_e$ and $\dot{\alpha}$ gives

$$\dot{\tau}_e = [G_t\cos\alpha]\dot{\gamma}, \quad \dot{\alpha} = \left[1 - \frac{G}{\tau_e}\sin\alpha\right]\dot{\gamma}. \tag{37}$$

Eliminating $\dot{\gamma}$ leads to the following differential equation

$$(\tau_e - G\sin\alpha)d\tau_e - (\tau_e G_t\cos\alpha)d\alpha = 0. \tag{38}$$

Using the standard techniques for solving linear first-order ordinary differential equations (Birkhoff and Rota, 1960), and taking into account the condition (35) at incipient plastic flow, we obtain the following solution:

$$\alpha(\tau_e) = \sin^{-1}\left\{\frac{1}{I(\tau_e)}\left[\int_{\tau_Y}^{\tau_e}\frac{I(\tau_e)}{G_t}\,d\tau_e + \frac{\tau_Y}{2G}\right]\right\}, \tag{39}$$

where

$$I(\tau_e) = \exp\left[\int_{\tau_Y}^{\tau_e}\frac{G}{G_t\tau_e}\,d\tau_e\right]. \tag{40}$$

At initial yield we have $\alpha = \alpha_Y = \sin^{-1}(\tau_Y/2G)$.

Given the equivalent shear stress—shear strain relation for the material, we substitute $G_t(\tau_e)$ in (40) and (39) to obtain $\alpha(\tau_e)$. Using (37), we then relate τ_e to the shear deformation γ as follows:

$$\gamma(\tau_e) = \gamma_Y + \int_{\tau_Y}^{\tau_e}\frac{1}{G_t\cos\alpha}\,d\tau_e. \tag{41}$$

The stress deviator components at this shear deformation γ are obtained from (36).

For a linear hardening material with $G_t = h = \text{const.}$, (39) can be integrated explicitly. This gives

$$\alpha(\tau_e) = \sin^{-1}\left\{\frac{\tau_e}{G+h}\left[1 - \frac{1}{2}\left(1 - \frac{h}{G}\right)\left(\frac{\tau_e}{\tau_Y}\right)^{-(1+G/h)}\right]\right\}. \tag{42}$$

For the solid bar subjected to a shear deformation $\gamma(R) \equiv \Gamma$ at its outer radius, we get from (9), (10), and (36) the resultant axial force and torque

$$F(\Gamma) = -\frac{3\pi R^2}{\Gamma^2}\int_0^\Gamma \gamma\tau_e(\gamma)\sin\alpha\,d\gamma$$

$$T(\Gamma) = \frac{2\pi R^3}{\Gamma^3}\int_0^\Gamma \gamma^2\tau_e(\gamma)\cos\alpha\,d\gamma. \tag{43}$$

From (8) and (36) the hydrostatic pressure distribution is

$$p(r) = \int_r^R \frac{1}{r}\,\tau_e(\gamma)\sin\alpha\,dr. \tag{44}$$

The normal stresses in the bar are obtained from (4).

For rigid plastic behavior, (14) leads to the classical solution (Nadai, 1950) according to which $\gamma_e = \gamma$ and the only nonzero stress component is $\sigma_{z\theta} = \tau_e$. This corresponds to $\alpha = 0$ in the foregoing elastic-plastic solution, and now $p = F = 0$. For an equivalent shear stress—shear strain curve of the form

$$\tau_e = f(\gamma_e), \tag{45}$$

the resulting twisting couple is

$$T(\Gamma) = \frac{2\pi R^3}{\Gamma^3}\int_0^\Gamma \gamma^2 f(\gamma)d\gamma. \tag{46}$$

4.2 Kinematic Hardening J_2 Flow Theory. In this case analytical solutions are readily obtained for the rigid-plastic model (22), (23). The solution in simple shear is such that all components of s_{ij} and β_{ij} are zero, except for those in the $\theta - z$ plane. Since $\dot{\gamma}_c = \dot{\gamma}$, (1) and (22) give

$$s_{\theta\theta} = \beta_{\theta\theta} = -s_{zz} = -\beta_{zz},$$

$$s_{z\theta} = \sigma_{z\theta} = \tau_Y + \beta_{z\theta}. \tag{47}$$

Form the shift rule (23), we get

$$\dot{\beta}_{\theta\theta} = -\dot{\beta}_{zz} = 2\beta_{z\theta}\overset{*}{\omega}$$

$$\dot{\beta}_{z\theta} = G_t\dot{\gamma} - 2\beta_{\theta\theta}\overset{*}{\omega}, \tag{48}$$

where $\overset{*}{\omega} = \Omega_{\theta z} = -\Omega_{z\theta}$ represents the components of the antisymmetric spin tensor Ω appearing in the definition (13) of the Jaumann rate. (All other $\Omega_{ij} = 0$ here.)

According to Tvergaard's (1978) model, the material spin ω (1) is employed in (13). As a result, $\overset{*}{\omega} = \dot{\gamma}/2$ and (48) can be written as

$$\dot{\beta}_{\theta\theta} = \beta_{z\theta}\dot{\gamma}, \quad \dot{\beta}_{z\theta} = (G_t - \beta_{\theta\theta})\dot{\gamma}. \tag{49}$$

In a manner analogous to (36), we introduce a parametric angle α as follows:

$$\beta_{\theta\theta} = \beta_e\sin\alpha, \quad \beta_{z\theta} = \beta_e\cos\alpha. \tag{50}$$

(Recall $\tau_e = \tau_Y + \beta_e$.) Substituting (50) into (49) gives (c.f. equations (37) and (38))

$$\dot{\beta}_e = [G_t\cos\alpha]\dot{\gamma}, \quad \dot{\alpha} = \left[1 - \frac{G_t}{\beta_e}\sin\alpha\right]\dot{\gamma} \tag{51}$$

$$(\beta_e - G_t\sin\alpha)d\beta_e - (\beta_e G_t\cos\alpha)d\alpha = 0. \tag{52}$$

Using a procedure similar to that used to solve (37) and (38) we obtain the following solution to (52)

$$\alpha(\beta_e) = \sin^{-1}\left[\frac{1}{\beta_e}\int_0^{\beta_e}\frac{\beta_e}{G_t}\,d\beta_e\right]. \tag{53}$$

Also, from (51),

$$\gamma(\alpha) = \int_0^\alpha\left[1 - \frac{G_t}{\beta_e}\sin\alpha\right]^{-1}d\alpha. \tag{54}$$

For a rigid-plastic power-law hardening material with an effective shear stress—shear strain curve of the form

$$\tau_e = \tau_Y + h\gamma_e{}^N \tag{55}$$

where h and N are constants, the above expressions give

$$\alpha = \frac{\gamma}{N+1}, \quad \beta_e = h\left[(N+1)\sin\left(\frac{\gamma}{N+1}\right)\right]^N. \tag{56}$$

From (47), (50), and (56) we immediately get the expressions for $\beta_{ij}(\gamma)$ and $s_{ij}(\gamma)$.

For the corresponding solid bar, the resultant torque and axial force for $\gamma(R) = \Gamma$ become

$$T(\Gamma) = \frac{2\pi R^3}{\Gamma^3}\int_0^\Gamma \gamma^2\left[\tau_Y + \beta_e\cos\left(\frac{\gamma}{N+1}\right)\right]d\gamma \tag{57}$$

and

$$F(\Gamma) = -\frac{3\pi R^2}{\Gamma^2}\int_0^\Gamma \gamma\beta_e\sin\left(\frac{\gamma}{N+1}\right)d\gamma, \tag{58}$$

respectively, with $\beta_e(\gamma)$ given by (56). From (8), (50), and (56) we obtain the following expression for hydrostatic pressure

$$p(r) = -\int_R^r \frac{1}{r}\beta_e \sin\left(\frac{\gamma}{N+1}\right) dr \tag{59}$$

where $\gamma = r\Gamma/R$. This result, combined with (4), gives the normal stresses across the bar for a given value of Γ.

For a linear hardening material ($N = 1$), we recover the simple shear solution given by Dafalias (1983); i.e., the above relations reduce to

$$\beta_{\theta\theta} = h(1-\cos\gamma), \quad \beta_{z\theta} = h\sin\gamma \tag{60}$$

$$s_{\theta\theta} = -s_{zz} = h(1-\cos\gamma)$$

$$s_{z\theta} = \sigma_{z\theta} = \tau_Y + h\sin\gamma.$$

For the solid bar we have

$$T(\Gamma) = \frac{2\pi R^3}{3}\left[\tau_Y + \frac{3h}{\Gamma^3}(2\Gamma\sin\Gamma + 2\cos\Gamma - \Gamma^2\cos\Gamma - 2)\right] \tag{61}$$

$$F(\Gamma) = -\frac{3\pi R^2 h}{\Gamma^2}\left[1 + \frac{\Gamma^2}{2} - \Gamma\sin\Gamma - \cos\Gamma\right]. \tag{62}$$

The kinematic hardening model proposed by Dafalias (1983) employs the spin $\dot{\mathbf{R}}\mathbf{R}^T$($\mathbf{R}$ is the orthogonal part of the polar decomposition of the velocity gradient), instead of the material spin ω, in the Jaumann rate expression (13). For simple shear deformations, this gives

$$\overset{*}{\omega} = \frac{2\dot{\gamma}}{\gamma^2 + 4} \tag{63}$$

in (48). Assuming linear hardening, the resulting equations can be solved explicitly for s_{ij} as functions of γ. The expressions for $s_{ij}(\gamma)$ can be found in (Dafalias, 1983) and shall not be repeated here. The transition from the simple shear solution to that for the solid circular bar is as described previously. We simply substitute the simple shear results $s_{ij}(\gamma)$ in (8)–(10) and (4) to determine the total stresses σ_{ij} across the bar, as well as the corresponding resultants F and T.

Among the numerous other kinematic-hardening models that have been proposed, many can be shown to lead to closed-form solutions for the large strain torsion of solid circular bars. If analytical solutions can be obtained for simple shear deformations, then the procedure outlined previously will provide the solution for the solid bar. The kinematic-hardening theories of Fressengeas and Molinari (1983), Dienes (1979) and Key (1984) give rise to such closed-form solutions.

4.3 Hypoelastic J_2 Deformation Theory. Because of the similarity between the elastic-plastic isotropic-hardening J_2 flow theory law (15) and the hypoelastic J_2 deformation theory relation (24), putting $G = G_s$ in the solution derived in Section 4.1 immediately furnishes the torsion solution for a material obeying the hypoelastic version (Stören and Rice, 1975) of J_2 deformation theory. Thus, equations (39)–(41) apply, but with G replaced by the secant shear modulus $G_s(\tau_e)$ as determined by the equivalent shear stress—shear strain relation for the material.

In the elastic range ($\gamma \le \gamma_Y$), the response is again given by (34). The elastic-plastic solution is simplified considerably by substituting $G_t = d\tau_e/d\gamma_e$, $G_s = \tau_e/\gamma_e$ and expressing the result in terms of γ_e. This leads to the result

$$\alpha = \sin^{-1}\left(\frac{\gamma_e}{2}\right), \quad \gamma = 2\alpha = 2\sin^{-1}\left(\frac{\gamma_e}{2}\right). \tag{64}$$

Substituting this in (36) gives

$$s_{\theta\theta} = -s_{zz} = 2G_s(\gamma_e)\sin^2\left(\frac{\gamma}{2}\right), \quad s_{z\theta} = G_s(\gamma_e)\sin\gamma. \tag{65}$$

Note that, from (35) and (64), the effective strain at yield satisfies $\gamma_{eY} = \tau_Y/G$.

For the solid bar (8)–(10) together with the above give

$$p(r) = -\int_R^r \frac{2}{r} G_s(\gamma_e)\sin^2\left(\frac{\gamma}{2}\right) dr \tag{66}$$

with $\gamma = r\Gamma/R$,

$$F(\Gamma) = -\frac{3\pi R^2}{\Gamma^2}\int_0^\Gamma 2\gamma G_s(\gamma_e)\sin^2\left(\frac{\gamma}{2}\right) d\gamma \tag{67}$$

and

$$T(\Gamma) = \frac{2\pi R^3}{\Gamma^3}\int_0^\Gamma \gamma^2 G_s(\gamma_e)\sin\gamma\, d\gamma. \tag{68}$$

In all of the foregoing expressions, G_s is evaluated at $\gamma_e = 2\sin(\gamma/2)$.

4.4 Hyperelastic J_2 Deformation Theory. The solution associated with the hyperelastic version of J_2 deformation theory (Hutchinson and Neale, 1987a) entails a calculation of the principal stretches λ_i and principal directions of Eulerian strain. For simple shear deformations, the principal stretches in the plane of shear are easily shown to be

$$\lambda_I = \frac{1}{\lambda_{II}} = \frac{\gamma}{2} + \left[1 + \frac{\gamma^2}{4}\right]^{1/2}. \tag{69}$$

The direction normal to this plane, ϵ_r, is also a principal direction and $\lambda_{III} \equiv \lambda_r = 1$. The direction of major principal Eulerian strain is inclined at an angle $\phi = \tan^{-1}(\lambda_{II})$ relative to the $\mathbf{e}_\theta$-axis, and the principal stress deviators, from (25), become

$$s_I = -s_{II} = 2G_s \ln\lambda_I, \quad s_{III} = s_{rr} = 0. \tag{70}$$

We also have

$$\tau_e = s_I, \ \gamma_e = 2\epsilon_I = 2\ln\lambda_I. \tag{71}$$

Transforming (70) from the principal Eulerian directions to the $\Theta - z$ reference axes gives the following components:

$$s_{\theta\theta} = -s_{zz} = \frac{2\gamma}{\sqrt{(4+\gamma^2)}} G_s \ln\lambda_I$$

$$s_{z\theta} = \frac{4}{\sqrt{(4+\gamma^2)}} G_s \ln\lambda_I \tag{72}$$

For the solid bar subjected to a twist $R\psi = \Gamma = \gamma(R)$, the resulting twisting couple becomes

$$T(\Gamma) = \frac{2\pi R^3}{\Gamma^3}\int_0^\Gamma \frac{4\gamma^2}{\sqrt{(4+\gamma^2)}} G_s \ln\lambda_I d\gamma, \tag{73}$$

and the axial force is

$$F(\Gamma) = -\frac{3\pi R^2}{\Gamma^2}\int_0^\Gamma \frac{2\gamma^2}{\sqrt{(4+\gamma^2)}} G_s \ln\lambda_I d\gamma. \tag{74}$$

Note that the torque and axial force satisfy the relation

$$\frac{F}{T} = -\frac{3\Gamma}{4R}. \tag{75}$$

The hydrostatic pressure distribution across the bar is

$$p(r) = \int_r^R \frac{2G_s\gamma}{r\sqrt{(4+\gamma^2)}} \ln\lambda_I dr \tag{76}$$

with $\gamma = r\Gamma/R$. Again, combining this result with (4) gives the normal stresses in the bar as a function of Γ.

4.5 Rate-Dependent Plasticity Laws. The rate-dependent constitutive model (28) leads to the following simple solution for shear:

$$\sigma_{z\theta} = \tau_e, \quad \dot{\gamma}_e = \dot{\gamma}, \tag{77}$$

with all other components of $s_{ij} = 0$. Thus, for the solid bar the hydrostatic pressure p, normal stress components σ_{ij}, and axial force F, are all zero.

For a bar twisted at a rate such that $\dot{\gamma}(R)=\dot{\Gamma}$, the relation (28) implies that, at a radial distance r,

$$\sigma_{z\theta}=K\gamma^N\dot{\gamma}^m, \tag{78}$$

with $\gamma(r)=r\Gamma/R$. Substituting this in (6) gives

$$T(\Gamma,\dot{\Gamma})=\frac{2\pi R^3}{(3+N+m)}K\Gamma^N\dot{\Gamma}^m. \tag{79}$$

For rate-independent behavior ($m=0$) and a power-law hardening curve of the form $\tau_e=K\gamma_e^N$, (79) becomes a special case of the classical rigid-plastic result (46).

5 Numerical Results and Discussion

In order to illustrate the differences in the responses predicted by the various rate-independent plasticity laws, the analytical solutions of the previous section are applied to materials whose uniaxial response is represented by a power-law relation of the type:

$$\frac{\tau_e}{\tau_Y}=\left(\frac{G}{\tau_Y}\right)\gamma_e \quad ; \quad \gamma_e\le\gamma_{eY}=\frac{\tau_Y}{G}$$

$$\frac{\tau_e}{\tau_Y}=1+K(\gamma_e-\gamma_{eY})^N \quad ; \quad \gamma_e\ge\gamma_{eY}. \tag{80}$$

This representation includes the linear hardening case when $N=1$. The rigid plastic versions are obtained by taking $\gamma_{eY}=0$. Figure 1 shows the $\tau_e-\gamma_e$ curve employed here: (a) a linear hardening law with $G/\tau_Y=500$, $K=0.5$, $N=1$, and (b) a power-law relation with $G/\tau_Y=500$, $K=2.845$, $N=0.2$. To deal with possible negative values of γ_e, we assume that the $\tau_e-\gamma_e$ curves are symmetric with respect to the origin.

The simple shear and torsion responses according to the linear hardening law are shown in Figs. 2(*a*)–2(*d*), while those pertaining to power-law hardening are described by Figs. 3(*a*)–3(*d*). The simple shear results consist of the graphs of the normalized shear and axial stresses ($s_{z\theta}/\tau_y$ and s_{zz}/τ_y assuming zero hydrostatic pressure) as functions of γ. The torsion results are described by the variation of the mean shear stress and axial stress (τ/τ_Y and σ/τ_Y) with respect to Γ. These variables are related to the torque and axial force through equations (9) and (10) as follows:

$$\tau=\frac{3T}{2\pi R^3}=\frac{3}{\Gamma^3}\int_0^\Gamma\gamma^2 s_{z\theta}(\gamma)d\gamma \tag{81}$$

$$\sigma=\frac{F}{\pi R^2}=-\frac{3}{\Gamma^2}\int_0^\Gamma\gamma s_{\theta\theta}(\gamma)d\gamma. \tag{82}$$

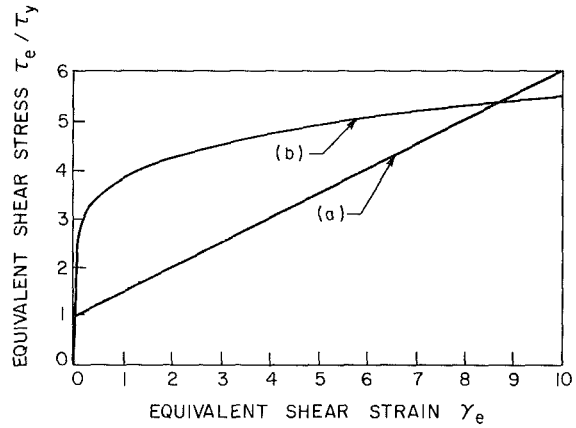

Fig. 1 Material models: (*a*) linear hardening, (*b*) power-law hardening

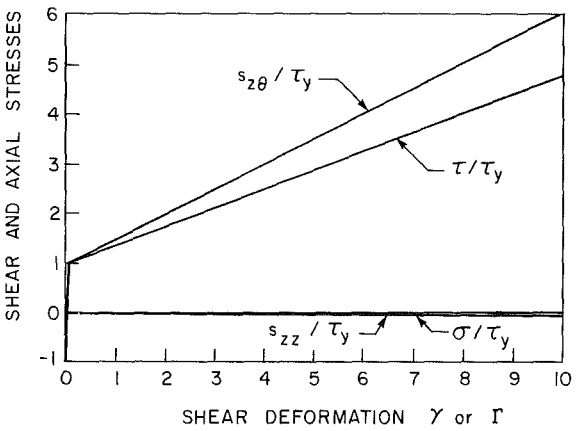

Fig. 2(*a*) Predicted responses in simple shear and torsion for J_2 isotropic-hardening theory (linear hardening)

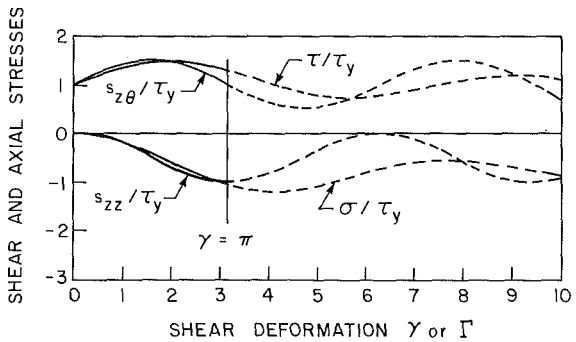

Fig. 2(*b*) Predicted responses in simple shear and torsion for J_2 kinematic-hardening theory (linear hardening)

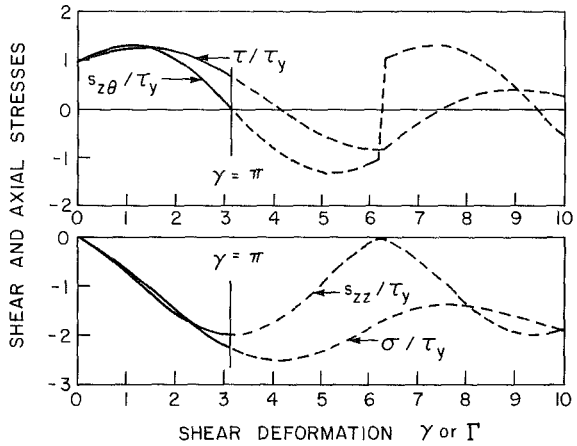

Fig. 2(*c*) Predicted responses in simple shear and torsion for J_2 hypoelastic theory (linear hardening)

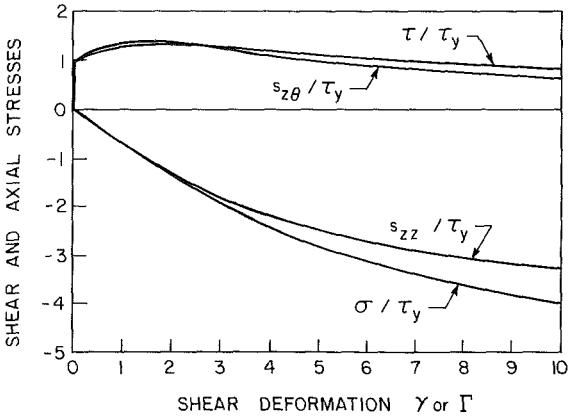

Fig. 2(*d*) Predicted responses in simple shear and torsion for J_2 hyperelastic theory (linear hardening)

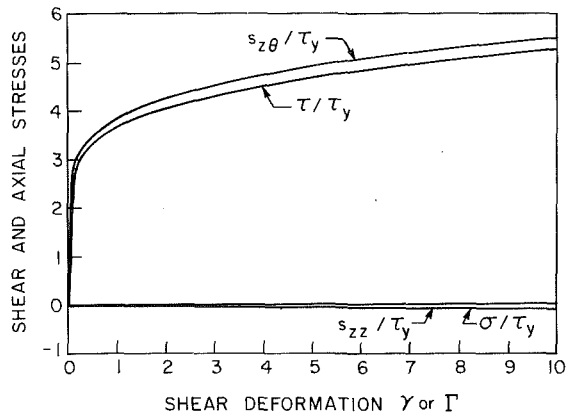

Fig. 3(a) Predicted responses in simple shear and torsion for J_2 isotropic-hardening theory (power-law hardening)

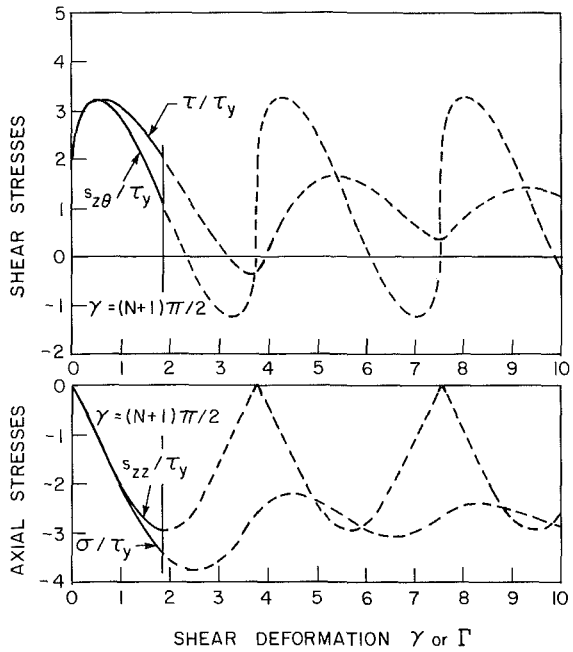

Fig. 3(b) Predicted responses in simple shear and torsion for J_2 kinematic-hardening theory (power-law hardening)

For simplicity, we do not show the radial distributions of σ_{rr}, σ_{zz}, $\sigma_{\theta\theta}$ in the twisted bar although, in the present case of fixed-end torsion, the radial variation of $\sigma_{z\theta}$ at any Γ can be inferred from the simple shear $s_{z\theta}-\gamma$ graph.

The results shown are for elastic-plastic material response, except those for the kinematic-hardening theory (Figs. 2(*b*) and 3(*b*)) which are obtained by treating the material as rigid plastic. In any case, since the elastic modulus is high ($G/\tau_y = 500$), the elastic-plastic results are very close to the rigid-plastic ones. Table 1 lists the rigid plastic solutions and their properties for simple shear and torsion assuming a rigid-plastic power-law material. Explicit closed-form expressions for τ and σ, although not listed here, can be obtained easily for the linear hardening material (for example, equations (61) and (62) for the kinematic hardening theory). Qualitatively, some of the results shown are similar to those reported in earlier work (Neale and Shrivastava 1985, 1989) except that previously they were obtained numerically. The dotted portions of the graphs indicate the regions for which the validity of the solutions is questionable on physical grounds as will be discussed later.

Table 1 may be used in conjunction with Figs. (2) and (3) for comparing the solutions from different theories, observing

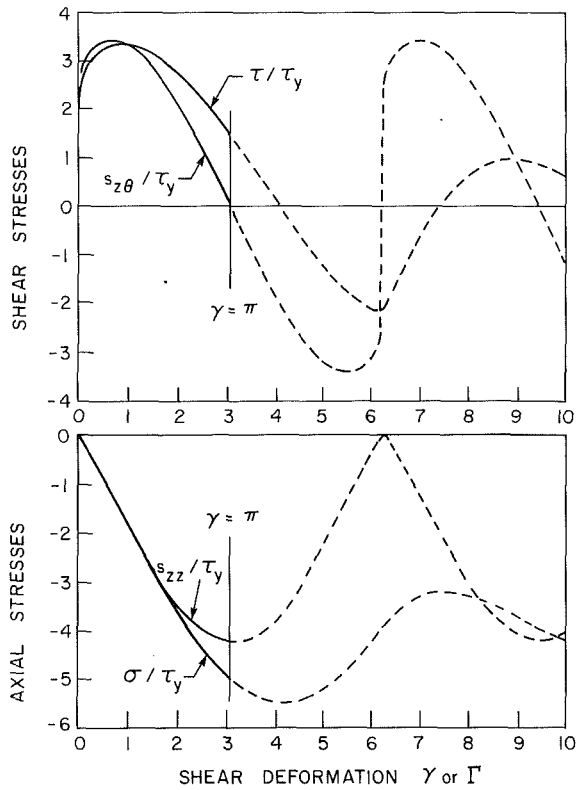

Fig. 3(c) Predicted responses in simple shear and torsion for J_2 hypoelastic theory (power-law hardening)

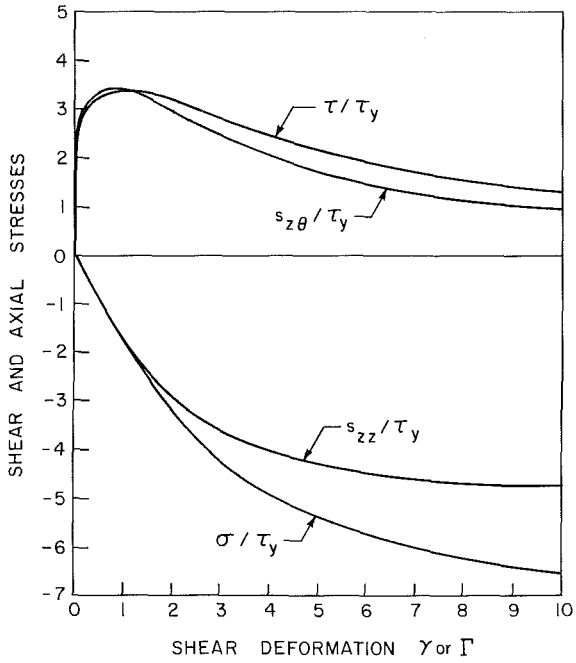

Fig. 3(d) Predicted responses in simple shear and torsion for J_2 hyperelastic theory (power-law hardening)

that essentially there are no qualitative differences in the responses with respect to the material models—linear or power law—and that we may consider the two sets of results together in the following discussion. We note first of all that both J_2 kinematic-hardening (Figs. 2(*b*) and 3(*b*)) and J_2 hypoelastic (Figs. 2(*c*) and 3(*c*)) theories predict periodic responses in simple shear, and hence oscillatory responses in torsion. The period is 2π for the hypoelastic theory and $(N+1)\pi$ for the kinematic-hardening theory. In contrast, the results obtained

Table 1 Predicted responses for a rigid plastic power-law material, $\tau_e/\tau_Y = f(\gamma_e) = [1 + K\gamma_e^N]$, in simple shear and fixed-end torsion

Variable	J_2 isotropic	J_2 kinematic	J_2 hypoelastic	J_2 hyperelastic
		SIMPLE SHEAR		
γ_e	γ	$(N+1)\sin\frac{\gamma}{(N+1)}$	$2\sin\frac{\gamma}{2}$	$2\,\text{an}(\frac{\gamma}{2}+[1+\frac{\gamma^2}{4}]^{\frac{1}{2}})$
s_{zz}/τ_Y	0	$-[f(\gamma_e)-1]\sin\frac{\gamma}{(N+1)}$	$-f(\gamma_e)\sin\frac{\gamma}{2}$	$-f(\gamma_e)\tanh\frac{\gamma_e}{2}$
$s_{z\theta}/\tau_Y$	$f(\gamma)$	$1+[f(\gamma_e)-1]\cos\frac{\gamma}{(N+1)}$	$f(\gamma_e)\cos\frac{\gamma}{2}$	$f(\gamma_e)\,\text{sech}\frac{\gamma_e}{2}$
		$(s_{z\theta}-\tau_Y=-\frac{ds_{zz}}{d\gamma})$	$(s_{z\theta}=-2f(\gamma_e)\frac{ds_{zz}}{d\gamma}/[(N+1)f(\gamma_e)-N])$	$(s_{z\theta}=\frac{-2s_{zz}}{\gamma})$
		TORSION		
σ/τ_Y	0	Eq.(82)	Eq.(82)	Eq.(82)
τ/τ_Y	$\frac{3f(\Gamma)+N}{N+3}$	Eq.(81)	Eq.(81)	Eq.(81)
		$(\tau-\tau_Y=-\frac{d\sigma}{d\Gamma})$		$(\tau=-\frac{2\sigma}{\Gamma})$

Table 2 Maximum $s_{z\theta}$ in simple shear and maximum τ in torsion and the corresponding s_{zz}, γ, and σ, Γ values for linear and power-law materials. (There is no maximum for isotropic hardening theory; the values given for this theory correspond to the maxima of the hyperelastic theory.)

Material Law	Simple Shear			Torsion		
Linear	max.$s_{z\theta}/\tau_Y$	γ	s_{zz}/τ_Y	max.τ/τ_Y	Γ	σ/τ_Y
Kine. Hardening	1.50	1.57	-0.50	1.46	2.0	-0.6
Hypoelastic	1.30	1.0	-0.71	1.28	1.3	-0.9
Hyperelastic	1.35	1.5	-1.02	1.34	1.9	-1.27
(Iso. Hardening	1.75	1.5	-0.006	1.71	1.9	-0.008)
Power-law	max.$s_{z\theta}/\tau_Y$	γ	s_{zz}/τ_Y	max.τ/τ_Y	Γ	σ/τ_Y
Kine. Hardening	3.25	0.5	-0.99	3.22	0.6	-1.17
Hypoelastic	3.42	0.7	-1.25	3.38	0.9	-1.59
Hyperelastic	3.44	0.8	-1.38	3.41	1.0	-1.71
(Iso. Hardening	3.72	0.8	-0.024	3.67	1.0	-0.033)

from the J_2 isotropic hardening (Figs. 2(*a*) and 3(*a*)) and J_2 hyperelastic (Figs. 2(*d*) and 3(*d*)) theories show mostly a monotonic variation, except that the shear stress or the torque for the hyperelastic material first rises to a maximum and then decreases monotonically.

We find that in all cases the axial stress (s_{zz} or σ) remains compressive. For a given γ or Γ it turns out to be the largest for the hyperelastic case. On the other hand, it remains negligibly small in the isotropic hardening case, thereby rendering the calculated response as approximately a pure shear one. For the kinematic-hardening and hypoelastic cases the s_{zz} stress component in simple shear varies periodically attaining a minimum value equal to zero. But in torsion, the stress σ corresponding to the axial force shows an attenuated variation with Γ.

Regarding the shear stress $s_{z\theta}$ in simple shear we note that, according to the hypoelastic theory, it undergoes a sign change at intervals of $\gamma = \pi$ regardless of the particular hardening law. The sign changes in $s_{z\theta}$ may or may not occur for the kinematic-hardening theory depending on the values of K and N in the power-law expression. The resulting torque from both of these theories, represented by the variation of τ, can also undergo sign changes depending on the material characteristics. It is evident that in the cases of hyperelastic and isotropic hardening theories, $s_{z\theta}$ and τ do not change sign and thus remain positive, though they do possess maximum values for the hyperelastic case.

It is interesting to observe that the initial responses in terms of shear stress are quite similar for the different theories (except for the isotropic hardening theory) and that the initial maximums of $s_{z\theta}$ or τ are not too different from each other. Table 2 provides a comparison of these maximums for the different theories and material models, together with the corresponding γ or Γ and s_{zz} or σ values. From this table we also notice that the maximum value of $s_{z\theta}$ in simple shear is quite close in value to the maximum value of τ of torsion. These observations then suggest that, at least in the initial stage, the shear stress response is rather insensitive to the constitutive law, and measurements of torque or shear stress in experiments may not be relied upon to discriminate between the intrinsic material characteristics in this range. However, the differences in s_{zz} or σ are quite significant even in the initial state, and it seems that their measurements would provide a better indication of the material characteristics.

With regard to the question of the physical validity of the solutions, we note that the solutions must be in accordance with the condition of continued plastic loading. For incremental theories of plasticity (Neale, 1981), neglecting elastic strains, these consist in requiring that $\dot{W} = s_{ij}\dot{\epsilon}_{ij} \geq 0$ and $\dot{\tau}_e \geq 0$ for the isotropic hardening theory, and $\dot{W} = \bar{s}_{ij}\dot{\epsilon}_{ij} \geq 0$ and $\dot{\beta}_e \geq 0$ for the kinematic hardening theory. On the other hand, for deformation theories (Neale, 1981), we have the single criterion requiring that $\dot{\tau}_e \geq 0$. On the basis of these criteria, we find that the solutions for the J_2 isotropic hardening incremental theory and J_2 hyperelastic deformation theory are valid for the entire $(0 \leq \gamma \leq 10)$ range of deformation. However, this is not the case with the other two theories. In the case of J_2 hypoelastic deformation theory, the range of validity is $0 \leq \gamma \leq \pi$ regardless of any particular material model. In the case of J_2 kinematic-hardening incremental theory, this range depends on the exponent of the power-law relation and is given by $0 \leq \gamma \leq (N+1)\pi/2$. It is obvious that exactly the same restrictions in terms of Γ apply to the torsional responses computed from these theories. For γ or Γ values higher than the upper limits we find that $\dot{\tau}_e < 0$ for the hypoelastic theory, and $\dot{\beta}_e < 0$ for the kinematic-hardening theory. The analysis of responses beyond the upper limits requires a closer examination of the assumptions involved in constitutive modeling of these two theories.

So far we have given explicit formulae for the torque T and axial force F, in terms of the shear deformation Γ, for the various constitutive theories. We shall now develop relations so that the simple shear results $s_{ij}(\gamma)$ can be extracted directly from experimentally measured axial force and torque-twist curves.

From (9) and (10), it follows that

$$\frac{\partial T}{\partial \Gamma} = \frac{1}{\Gamma}[-3T + 2\pi R^3 s_{z\theta}(\Gamma)] \tag{83}$$

$$\frac{\partial F}{\partial \Gamma} = \frac{1}{\Gamma}[2F - 3\pi R^2 s_{\theta\theta}(\Gamma)]. \tag{84}$$

As a result, to extract the simple shear relations we use

$$s_{z\theta}(\Gamma) = \frac{1}{2\pi R^3}\left[3T + \Gamma\frac{\partial T}{\partial \Gamma}\right] \tag{85}$$

$$s_{\theta\theta}(\Gamma) = -s_{zz}(\Gamma) = \frac{1}{3\pi R^2}\left[2F - \Gamma\frac{\partial F}{\partial \Gamma}\right]. \tag{86}$$

Recall that all other $s_{ij} = 0$.

The relation (85) is identical to that derived by Nadai (1950) and Hill (1950) on the basis of J_2 flow theory. This expression and (86), however, hold for all of the constitutive models considered here. They can be used together with the theoretical results (e.g., those summarized in Table 1) to interpret ex-

perimental data and determine material constants in the large strain range. For improved accuracy at small Γ, it is preferable to write (85) as

$$s_{z\theta}(\Gamma)=\frac{1}{2\pi R^3}\left[\Gamma^2\frac{\partial(T/\Gamma)}{\partial\Gamma}+4T\right] \tag{87}$$

as suggested by Hill (1950) and Störakers (1979), and

$$s_{\theta\theta}(\Gamma)=-s_{zz}(\Gamma)=-\frac{\Gamma^3}{3\pi R^2}\frac{\partial(F/\Gamma^2)}{\partial\Gamma}. \tag{88}$$

Also, substituting the above expressions in (31) and using the results of Table 1 allows us to construct the effective shear stress (τ_e)-effective shear strain (γ_e) curves from the experimentally measured axial force and torque-twist curves.

We conclude this study with a brief discussion concerning experiments involving large strain torsion. Although the torsion test is widely used for simulating large strain behavior of metals, for example, in rolling, the body of test data documenting the development of axial forces or length changes with the progression of twist is rather sparse. Swift (1947) was the first to conduct large-strain torsion tests on solid circular bars and tubes of several metals at room temperature. These were free-end tests allowing length changes, and the maximum shear attained before failure was of the order of $\Gamma=6$. He observed that, with the exception of lead specimens which shortened, all other specimens exhibited monotonic length increases. This observation, in terms of fixed-end torsion, implies that at room temperature one can expect the development of an axial compressive force which increases with twist. At elevated temperatures, the situation appears to be quite different. For example, Hardwick and Tegart (1961) in their tests observed that although initially ($\Gamma<6$), the specimens showed a length increase, in agreement with Swift's observations, further twisting to ultra large strains ($\Gamma\approx 20$) produced a net shortening of all the specimens (with the exception of aluminum which, after initial lengthening, showed no further lengthening or shortening). Their fixed-end tests were also consistent with the above finding in that the compressive force developed initially changed to a tensile force at large shear strains (again with the exception of aluminum).

The more recent fixed-end tests reported by Montheillet, Cohen, and Jonas (1984) on aluminum, copper, and iron bar specimens have confirmed the findings of Hardwick and Tegart. The typical experimental torque and axial force versus twist curves (Figs. 1 and 3 of Montheillet et al.) show first that a common characteristic of the torque-twist curves is that the torque attains a single maximum at a relatively small shear strain, and thereafter it begins to drop to an almost steady-state value. On the other hand, they observe that the axial force is initially compressive and attains a maximum at about the same strain at which maximum torque is reached. Another trend is that as the test temperature increases, the value of the maximum compressive force diminishes. With further twist, past the maximum point, the axial force either decreases to a steady-state tension value or displays a limited oscillatory behavior in the sense of reaching a minimum and then again attaining a maximum. The attainment of a steady-state tension value seems possible only at high enough temperatures.

A qualitative comparison of these experimental observations with the corresponding predictions of the theories considered in this investigation makes it quite clear that none of the constitutive laws examined is capable of accurately simulating the experimental behavior for arbitrarily large strains. On the other hand, the moderately large strain behavior (up to the point of maximum torque) is well-described by any of the theories (except by the J_2 isotropic hardening theory which does not display a maximum).

Acknowledgments

This work was supported by the Natural Sciences and Engineering Research Council of Canada (NSERC) and the government of the Province of Québec (Programme FCAR).

References

Birkhoff, G., and Rota, G. C., 1969, *Ordinary Differential Equations*, Blaisdell Publishing Company, Waltham, Mass.

Budiansky, B., 1970, unpublished work, (see Hutchinson, 1973).

Dafalias, Y. F. 1983, "Corotational Rates for Kinematic Hardening at Large Plastic Deformations," ASME JOURNAL OF APPLIED MECHANICS, Vol. 105, pp. 561–565.

Dienes, J. K., 1979, "On the Analysis of Rotation and Stress Rate in Deforming Bodies," *Acta Mechanica*, Vol. 32, pp. 217–232.

Fressengeas, C., and Molinari, A., 1983, "Modèles d'écrouissage cinématique en grande déformation," *Comptes Rendus, Academie des Sciences,* Paris, Vol. 297, Séries II, pp. 93–96.

Hardwick, D., and Tegart, W. J., 1961, "La déformation des métaux et alliages par torsion à haute température," *Memoires scientifiques, Revue de metallurgie*, Vol. 8, pp. 869–880.

Hill, R., 1950, *The Mathematical Theory of Plasticity*, Oxford University Press, London.

Hill, R., 1970, "Constitutive Inequalities for Isotropic Elastic Solids Under Finite Strain," *Proceedings of the Royal Society, London*, Vol. A314, pp. 457–472.

Hutchinson, J. W., 1973, "Finite Strain Analysis of Elastic-Plastic Solids and Structures," *Numerical Solution of Nonlinear Structural Problems*, R. F. Hartung, ed., AMD Vol. 6, ASME, New York, pp. 17–29.

Hutchinson, J. W., and Neale, K. W., 1978a, "Sheet Necking—II. Time-Independent Behavior," *Mechanics of Sheet Metal Forming*, D. P. Koistinen and N.-M. Wang, eds., Plenum Press, New York, pp. 127–153.

Hutchinson, J. W., and Neale, K. W., 1978b, "Sheet Necking—III. Strain-Rate Effects," *Mechanics of Sheet Metal Forming,* D. P. Koistinen, and N.-M Wang, eds., Plenum Press, New York, pp. 269–285.

Key, S. W., 1984, "Theoretical Foundations for Large Scale Computations for Nonlinear Material Behavior," *Mechanics of Elastic and Inelastic Solids*, S. Nemat-Nasser, R. J. Asaro, and G. A. Hegemier, eds., Martinus Nijhoff Publishers, Amsterdam.

Lee, E. H., Mallett, R. L., and Wertheimer, T. B., 1983, "Stress Analysis for Anisotropic Hardening in Finite-Deformation Plasticity," ASME JOURNAL OF APPLIED MECHANICS, Vol. 50, 1983, pp. 554–560.

Montheillet, F., Cohen, M., and Jonas, J. J., 1984, "Axial Stresses and Texture Development During the Torsion Testing of Al, Cu and α-Fe," *Acta Metallurgica*, Vol. 32, pp. 2077–2089.

Nadai, A, 1950, *The Theory of Flow and Fracture of Solids*, McGraw-Hill, New York.

Nagtegaal, J. C., and De Jong, J. E., 1982, "Some Aspects of Non-Isotropic Workhardening in Finite Strain Plasticity," Proceedings of the Workshop on *Plasticity of Metals at Finite Strain: Theory Experiment and Computation*, E. H. Lee and R. L. Mallett, eds., Division of Applied Mechanics, Stanford University, Stanford, Calif., and Department of Mechanical Engineering, Aeronautical Engineering and Mechanics, Rensselaer Polytechnic Institute, Troy, N.Y., pp. 65–102.

Neale, K. W., 1981, "Phenomenological Constitutive Laws in Finite Plasticity," *Solid Mechanics Archives*, Vol. 6, pp. 79–128.

Neale, K. W., and Shrivastava, S. C., 1985, "Finite Elastic-Plastic Torsion of a Circular Bar," *Engineering Fracture Mechanics*, Vol. 21, pp. 747–754.

Neale, K. W., and Shrivastava, S. C., 1989, "Kinematic Work-Hardening Models and Their Implications on Large Strain Plastic Behaviour in Torsion," *Yielding, Damage and Failure of Anisotropic Solids,* J. P. Boehler, ed., Mechanical Engineering Publications, London, pp. 131–143.

Odqvist, F. K. G., 1966, *Mathematical Theory of Creep and Creep Rupture*, Clarendon Press, Oxford, U.K.

Störakers, B., 1979, "An Explicit Method to Determine Response Coefficients in Finite Elasticity," *Journal of Elasticity*, Vol. 9, pp. 207–214.

Stören, S., and Rice, J. R., 1975, "Localized Necking in Thin Sheets," *Journal of the Mechanics and Physics of Solids*, Vol. 23, pp. 421–441.

Swift, H. W., 1947, "Length Changes in Metals Under Torsional Overstrain," *Engineering*, Vol. 163, pp. 253–257.

Tvergaard, V., 1978, "Effect of Kinematic Hardening on Localized Necking in Biaxially Stretched Sheets," *International Journal of Mechanical Sciences*, Vol. 20, pp. 651–658.